PHYSICAL REVIEW B **108**, 214409 (2023)

Phase coexistence and nonequilibrium dynamics under simultaneously applied magnetic field and pressure: Possible role of the interface

Sudip Pal, Kranti Kumar, and A. Banerjee
UGC DAE Consortium for Scientific Research Khandwa road, University campus Indore-452001, Madhya Pradesh, India

(Received 17 May 2022; revised 9 January 2023; accepted 17 November 2023; published 11 December 2023)

Strong spin-lattice coupling makes external pressure (P) an important parameter across a first-order magnetostructural phase transition. Here, we have studied the effect of P under different magnetic fields on the phase coexistence and kinetics of nucleation and growth around such transitions in two prototype systems $Pr_{0.5}Ca_{0.5}Mn_{0.975}Al_{0.025}O_3$ and $La_{0.5}Ca_{0.5}MnO_3$, where the ferromagnetic-metal and antiferromagnetic-insulator phases compete in real space. We have determined the $H-P$ phase diagram of supercooling and superheating temperatures. The change in supercooling and superheating temperatures and the nucleation and growth control the phase coexistence. Surprisingly, despite having contrasting ground states, in both $Pr_{0.5}Ca_{0.5}Mn_{0.975}Al_{0.025}O_3$ and $La_{0.5}Ca_{0.5}MnO_3$ the transformation rate between the two states is suppressed at higher pressure. This proves that there must be some universal phenomena controlling the dynamics. Different spin and structural order at the interface of the two phases appear to be responsible for giving rise to strong frustration and eventually hindering the kinetics, resulting in the stabilization of glasslike behavior.

DOI: 10.1103/PhysRevB.108.214409

I. INTRODUCTION

Over the last two decades, first-order phase transition has received intense scientific attention and new phenomena have been found. In this context, various classes of materials, for instance, multiferroics showing strong magnetodielectric coupling, Mott insulators undergoing metal-insulating transition, artificial spin ice, etc., and of course manganites, shape memory alloys showing colossal magnetoresistance, magnetocaloric effects are under intensive scrutiny [1–6]. The two key features observed across the first-order transition are the phase coexistence and the slow dynamics across the transition [7–12]. Although there are studies on phase coexistence, investigation of the kinetics across transition and the quantitative analysis of phase coexistence is extremely limited. In addition, the role of strong spin-lattice coupling across first-order magnetostructural phase transitions is well known [13], which inevitably points towards the importance of hydrostatic pressure, where the sample is squished from every direction. However, the question of how hydrostatic pressure, particularly in the presence of a magnetic field, affects the phase coexistence and the dynamics across the first-order transition is scarce in the literature [14]. In this backdrop, manganites can serve as an excellent prototype [15–19].

Colossal magnetoresistance in manganites, large magnetocaloric and magnetostriction in various alloys and intermetallics are directly related to the coexistence of metallic-ferromagnetic (FM) and insulating-antiferromagnetic (AFM) phases appearing due to the first-order magnetic transition (FOMT) [20–22]. A first-order transition can be distinguished from a continuous transition by the appearance of supercooling $[H^*, T^*]$ and superheating $[H^{**}, T^{**}]$ lines which give rise to a hysteresis across the transition in the $H-T$ plane. However, in the presence of quenched disorder, $[H^*, T^*]$ and $[H^{**}, T^{**}]$ lines broaden into bands [23]. The broadening of supercooling and superheating bands results in phase coexistence of the two phases in the hysteresis region. Across the transition, one phase slowly transforms into another phase through the nucleation and growth process. In addition, it is observed in several materials that the kinetics of FOMT, i.e., the nucleation and growth process get arrested below a heuristic band, called the kinetic arrest band $[H_K, T_K]$. The transformation from the high-T phase to the low-T phase is arrested below that part of the $[H_K, T_K]$ band which lies above the $[H^*, T^*]$ band and the system below the thermal hysteresis remains as a composite of the transformed fraction of the low-T phase and the untransformed fraction of the high-T phase [24–32]. In our study, we have combined both H and P to study the phase coexistence and the dynamics of FOMT under pressure at different magnetic fields. We have focused on two well-known manganites $Pr_{0.5}Ca_{0.5}Mn_{0.975}Al_{0.025}O_3$ (PCMAO) and $La_{0.5}Ca_{0.5}MnO_3$ (LCMO) as representative phase-separated systems because these two systems have opposite ground states [25,27]. Upon cooling, PCMAO undergoes a phase transition from high-T CE type AFM to low-T FM phase. On the other hand, LCMO undergoes a transition from high-T FM to low-T CE type AFM phase.

Our aim is twofold: How does P influence the phase coexistence across the $H-T$ region where magnetization exhibits thermal hysteresis due to supercooling and superheating phenomena. Moreover, PCMAO and LCMO show phase coexistence even below the thermal hysteresis due to kinetic arrest of the first-order phase transition. Hence, we will probe the effect of P and H at the low-temperature regime below the hysteresis. Throughout the study, we emphasize an important fact that in both of these regions (across and below the thermal hysteresis), the phase coexistence is a nonequilibrium phenomenon and the timescale associated with the

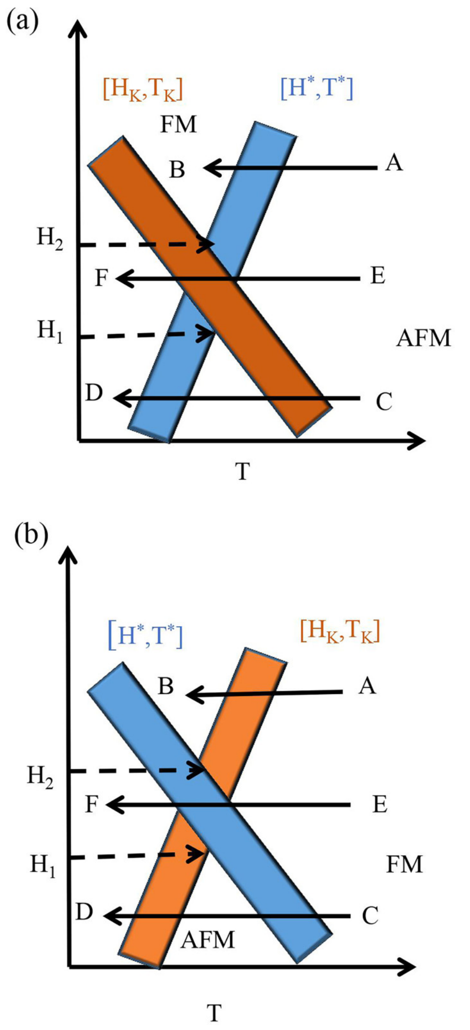

FIG. 1. Schematic band diagram of kinetic arrest in systems with (a) FM ground state, (b) AFM ground state. Here,the supercooling and kinetic arrest bands are shown in blue and orange color, respectively. Superheating band is not shown. Different arrows indicate cooling paths at different magnetic fields.

nonequilibrium dynamics can be tuned by H and P. In addition, a detailed quantitative understanding of the volume fraction of the coexisting phases is necessary to exploit the phase coexistence as a device in technological applications. Here, we have used bulk magnetization value to estimate the volume fraction of the FM-metal and AFM-insulator phases. It may be noted that until now mostly the surface sensitive techniques, like the Hall probe, scanning tunneling microscopy, magnetic force microscopy, photoelectron spectroscopy, etc., have been used as a probe of phase coexistence [3–6], but the surface often contains additional disorder and strain. As a result, the nature of the phase coexistence in the bulk may be different.

II. KINETIC ARREST IN PCMAO AND LCMO

The phenomena of kinetic arrest can be understood from Figs. 1(a) and 1(b), where we have shown the schematic band diagrams of kinetically arrested first-order phase transitions. Figure 1(a) is applicable in systems where the transition occurs between the high-T AFM and the low-T FM phase. PCMAO is in the paramagnetic state at room temperature and undergoes a second-order phase transition to the CE-type antiferromagnetic (AFM) phase with the decrease in temperature. The high-T AFM state is eventually followed by a FOMT to the low-T FM phase on further cooling. In the conversional FOMT, the transition is controlled by supercooling and superheating temperatures. However, it has been observed that several compounds which undergo FOMT show unusual properties primarily associated with the first-order transition. In particular, the low-T magnetic state shows interesting features, for example, metastability, cooling history dependence, etc. [24–32]. This anomalous magnetic response has been explained in the light of the kinetic arrest and the kinetic arrest temperature. It is also observed that the nature of the kinetic arrest phenomena critically depends on the ground state of the material. For example, the effect of kinetic arrest in PCMAO, where the ground state is FM, can be understood from the schematic in Fig. 1(a). If PCMAO is cooled in the presence of a magnetic field $H > H_2$ (path AB), it encounters the $[H^*, T^*]$ band before $[H_K, T_K]$ band, and hence undergoes the transition from high-T AFM to low-T FM phase. In this case, the low-temperature phase of PCMAO is FM. On the other hand, if PCMAO is cooled at $H < H_1$ (along path CD), it encounters $[H_K, T_K]$ band before $[H^*, T^*]$, and the transition is completely arrested. In this case, the transition from high-T AFM to low-T AFM does not occur and hence PCMAO stays in the AFM phase down to the lowest temperature. However, the AFM phase is metastable at low temperatures. When the sample is cooled at intermediate fields $H_1 < H < H_2$ (say along EF), the first-order transition is partially arrested, and we get phase coexistence of the AFM and FM phases which persists down to the lowest temperature even below the supercooling limit.

On the other hand, Fig. 1(b) is applicable in systems where the transition occurs between the high-T FM to the low-T AFM phase. LCMO is in the paramagnetic state at room temperature and undergoes a second-order transition to the FM phase with the decrease in temperature. The high-T FM state is eventually followed by a FOMT to low-T CE type AFM phase on further cooling. In this case, the effect of kinetic arrest on the system can be understood from the schematic in Fig. 1(b). If LCMO is cooled in presence of magnetic field $H > H_2$ (path AB), we first encounter the $[H_K, T_K]$ band before $[H^*, T^*]$ band, and hence the transition from high-T AFM to low-T FM phase is completely arrested. On the other hand, if it is cooled at $H < H_1$ (along path CD), we encounter the $[H^*, T^*]$ band before $[H_K, T_K]$, and the transition occurs. However, when the sample is cooled at intermediate fields $H_1 < H < H_2$ (say along EF), the transition is partially arrested, and we get an incomplete phase transition, and the coexistence of the FM and AFM phases persists down to the lowest temperature even below the supercooling limit. It should be noted here that aside from manganites, various other systems have been found to exhibit the signatures of kinetically arrested first-order transitions [33–38].

In this paper, first, we have used the temperature-dependent magnetization measurements under varying P and H to map the $[H^*, T^*]$, $[H^{**}, T^{**}]$, $[H_K, T_K]$ bands in $H - P - T$

landscape. In addition, we have estimated the volume fraction of FM and AFM phases at low temperature ($T = 5$ K) at different P and H, which is a result of kinetic arrest. Finally, we have carried out time-dependent magnetization measurements to address the effect of pressure on the dynamics, i.e., the nucleation and growth process. In this case, we have focused on both regions, i.e., across the first-order transition, where thermal hysteresis exists. Also, we have probed at low temperature, below the thermal hysteresis. We found that the interface of the FM and CE type AFM phase plays a crucial role in controlling the dynamics in these two systems. To further confirm whether there is any role of interfacial coupling at the FM-AFM interface, we investigated the field-cooled $M - H$ loop to look for the exchange-bias effect.

III. EXPERIMENTAL DETAILS

Polycrystalline bulk samples of PCMAO and LCMO have been prepared by the standard solid-state method and chemical route, known as the pyrophoric method, respectively [27,39]. Further details on the sample preparation and characterization can be found in Refs. [27,39]. Magnetic measurements have been carried out in commercial 7-T superconducting quantum interference device (SQUID) magnetometer (M/S Quantum Design, USA). For the measurements under pressure, a Cu-Be cell (Mcell 10, easy laboratory) has been used, where a fixed pressure was applied and locked at room temperature. The pressure cell can be mounted inside the magnetometer to carry out the magnetization measurements, which have been performed at different H at a fixed pressure. Daphne oil has been used as the pressure-transmitting medium to maintain the hydrostatic condition of pressure on the sample. Pressure values have been determined from the variation of superconducting transition temperature of Sn wire that has been loaded inside the pressure cell [28]. Field-cooled cooling (FCC) magnetization (M) versus T curves are recorded while cooling the sample in presence of a constant magnetic field. The field-cooled warming (FCW) curves are recorded in the subsequent warming cycle without changing the field. For zero-field-cooled (ZFC) measurements, the sample has been cooled down to $T = 5$ K in the absence of external field. Then, M versus T data have been recorded during warming after applying external field at the lowest temperature. Time- (t-) dependent magnetization (M) data have been recorded in field-cooling (FC) mode where the sample is first cooled from $T = 320$ K to the measurement temperature in the presence of the external field. After the temperature becomes stable, the isothermal variation of M with time has been recorded keeping the field unchanged. The sample cooling and heating rate is 1.5 K/min.

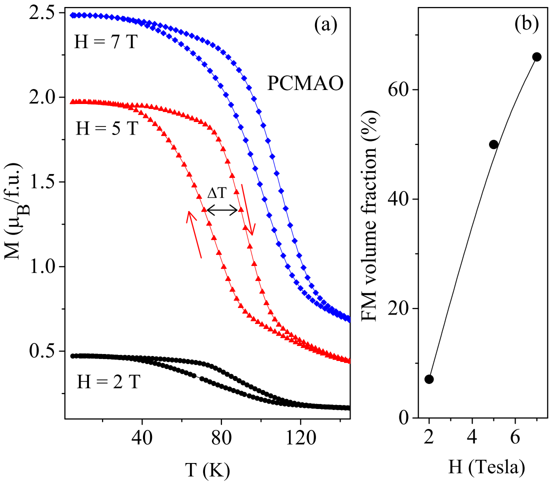

FIG. 2. (a) Temperature variation of magnetization of PCMAO at $H = 2$, 5 and 7 T recorded in FCC and FCW modes. The thermal hysteresis indicates the transition between high-T AFM and low-T FM phases and it shifts towards higher temperature with magnetic field. ΔT is the width of the thermal hysteresis. (b) Variation of FM volume fraction (f_{FM}) with H at $T = 5$ K. The line is a guide to eye.

IV. RESULTS

Figure 2(a) presents the temperature variation of M (FCC and FCW) across the transition between high-T AFM and low-T FM phases in PCMAO at three different magnetic fields. Magnetization shows thermal hysteresis across the transition and the hysteresis shifts towards higher temperature with increase in H. Also note that the width of the thermal hysteresis ([ΔT, see Fig. 2(a)] varies nonmonotonically with H. At $H = 5$ T, the width $\Delta T \approx 20$ K, which is significantly larger than $\Delta T \approx 12$ and 10 K at $H = 2$ and 7 T, respectively. On the other hand, the value of M at low temperatures, say at $T = 5$ K, increases by a large amount with increase in H which can be explained from the schematic shown in Fig. 1(a) [25]. As the measurement field increases, the volume fraction of the FM phase increases, which results into higher magnetization value at low temperature.

It should be mentioned here that the saturation field of the FM phase in PCMAO is a few hundred Oe [25]. At low temperature, the system contains both FM and AFM volume fractions, and the amount of the FM phase increases with H at the expense of the competing AFM phase [25]. In Fig. 2(b), we have estimated the variation of the FM phase fraction at $T = 5$ K with the applied magnetic field. It has been estimated from the magnetization value at $T = 5$ K ($M_{5\,\mathrm{K}}$) following the method described in Ref. [30]. If f_{FM} corresponds to the amount of the FM volume fraction at $T = 5$ K and the rest is AFM, so that (1-f_{FM}) corresponds to the AFM volume fraction, then $M_{5\,\mathrm{K}}$ is given by the relation

$$M_{5\,\mathrm{K}} = f_{\mathrm{FM}}(M_0 + \alpha H_m) + (1 - f_{\mathrm{FM}})\beta H_m. \qquad (1)$$

Here, α and β are the dc susceptibilities (dM/dH) of the FM and AFM phases, respectively, which are obtained from the slope of the $M - H$ curve at $T = 5$ K. M_0 is the spontaneous magnetization of the FM phase. The details of this procedure can be found in Ref. [30]. As H increases from $H = 2$ to 7 T, f_{FM} also increases by more than eightfold from around 7% to 60%.

In Figs. 3(a) and 3(b), we have shown the FCC and FCW curves of PCMAO and LCMO, respectively. Different curves correspond to the different applied pressure at a constant $H = 2$ and 1 T for PCMAO and LCMO, respectively. It may be mentioned here that a part of these data of LCMO has been reported earlier in Ref. [28] but has been reproduced here to make this paper self-content. The broad thermal hysteresis

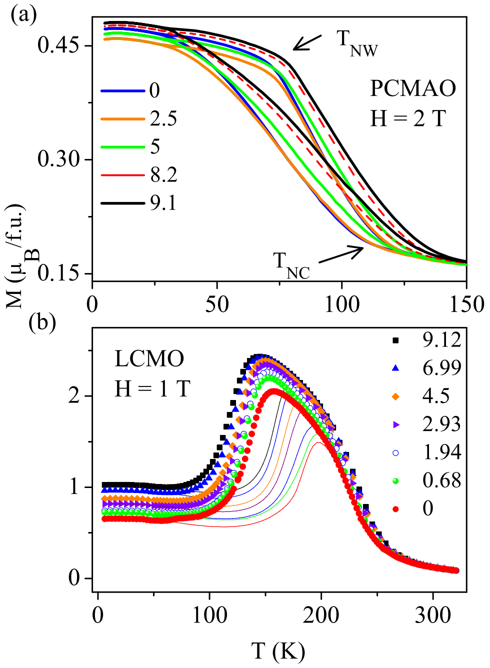

FIG. 3. Temperature variation of magnetization in different pressure of (a) PCMAO at $H = 2$ T. (b) LCMO at $H = 1$ T. The legends indicate the P values applied on the sample in the unit of kbar. In case of LCMO also, the transformation rate from high-T FM to low-T AFM phase can be found from the slope of the FCC curves at respected pressure values.

between the FCC and FCW curves evinces the coexistence of the high- and low-temperature phases across the hysteresis. Besides, due to kinetic arrest, the phase coexistence prevails down to the lowest temperature in both these systems. In PCMAO, the M at $T = 5$ K ($M_{5\,\mathrm{K}}$) shows nonmonotonic variation with pressure. It initially decreases as we increase the pressure from ambient to $P = 2.5$ kbar. As pressure increases further, $M_{5\,\mathrm{K}}$ starts to increase again. On the other hand in LCMO, $M_{5\,\mathrm{K}}$ monotonically increases with pressure. Such variation of $M_{5\,\mathrm{K}}$ indicates that the volume fraction of the two coexisting phases (FM and AFM) changes with pressure in both systems, but the dependence is qualitatively very much different. In the next section, we will estimate the volume fraction of the FM phase at $T = 5$ K in $H - P$ landscape and show that the efficiency of pressure in tuning the volume fraction of the coexisting phases also depends upon the applied magnetic field.

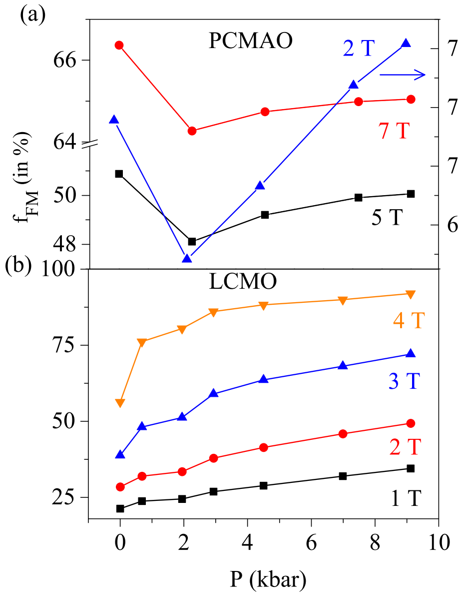

FIG. 4. Change in volume fraction of the metallic-FM phase (f_{FM}) with H and P in (a) PCMAO and (b) LCMO. Note that in case of PCMAO, f_{FM} initially decreases and finally starts to increase again with pressure. On the other hand in LCMO, f_{FM} monotonically increases.

A. Effect of pressure and magnetic field on the FM and AFM phase fractions at low temperature

In Figs. 4(a) and 4(b), we present the variation of the FM volume fraction (f_{FM} in %) at $T = 5$ K in PCMAO and LCMO, respectively, at different P and H, which we have calculated using Eq. (1). It is interesting that in case of PCMAO [Fig. 4(a)], pressure initially suppresses the FM phase fraction. At higher pressure, f_{FM} increases again. Moreover, the change in phase fraction with the application of pressure is small. For example [see $H = 5$ T, Fig. 4(a), black filled square], at $H = 5$ T f_{FM} is around 50.8% at ambient pressure which is consistent with Fig. 2(b). As pressure is increased to $P = 2.5$ kbar, f_{FM} reduces to $f_{\mathrm{FM}} = 48\%$ which is followed by monotonic rise to 50.1% at $P = 9.1$ kbar. Such kind of nonmonotonic dependence of f_{FM} on pressure is interesting. It points towards the existence of two competing mechanisms occurring simultaneously, one trying to enhance the f_{FM} and the other mechanism tending to reduce the f_{FM} at each pressure. As we will show later that this is actually the situation and the net volume fraction of the two phases is decided by which of these two mechanisms is dominant. On the other hand, in case of LCMO as shown in Fig. 4(b), the change in the FM volume fraction is comparatively large and it monotonically increases with increase in the pressure. For example, at $H = 1$ T, $f_{\mathrm{FM}} = 21.1\%$ at ambient pressure which monotonically rises to 34.5% at $P = 9.12$ kbar. Also note that at low fields say $H = 1$ T, f_{FM} varies rather smoothly as a function of pressure. However, at higher H, say 4 T, f_{FM} initially increases sharply and tends to saturate with increase in the applied pressure. We note here that in the phase coexistence region, if only external magnetic field is increased at ambient pressure, then it is straightforward to expect that magnetic field will always enhance the volume fraction of FM phase. However, in case of pressure, it monotonically increases the f_{FM} in LCMO, and in PCMAO it exhibits nonmonotonic trend. It indicates that in the phase coexistence region at low temperature the change in volume fraction of the competing metallic-FM and insulating-AFM phases with external pressure in both PCMAO and LCMO is qualitatively different. Moreover, the variation of the volume fraction is quantitatively much different: in PCMAO the change is much smaller than in LCMO. Therefore, the effect of pressure on phase coexistence is not so straightforward. To fully understand the dependence of volume fraction with

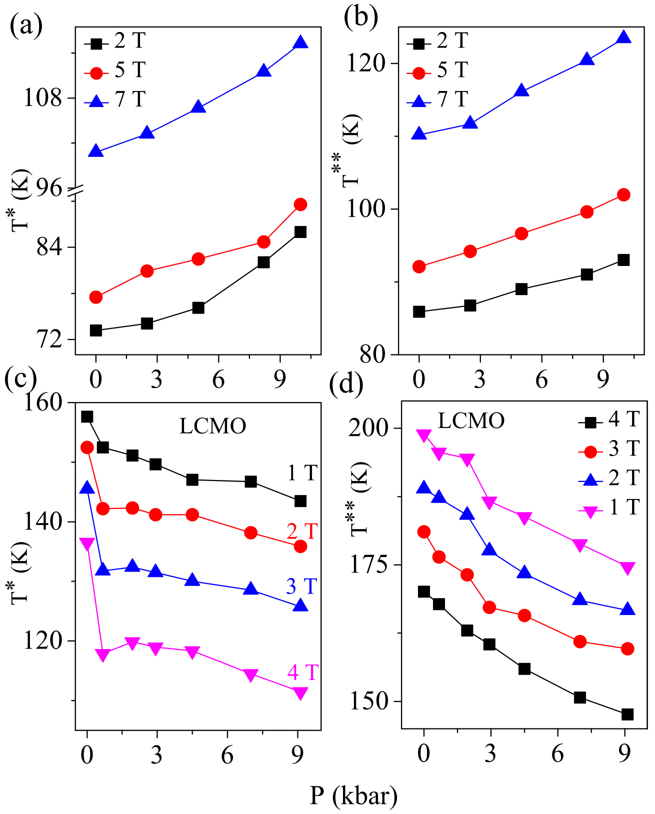

FIG. 5. (a), (b) Show the variation of the T^* and T^{**} with P at different applied field in PCMAO. (c), (d) Show the same in case of LCMO. The solid lines are guide to eye.

pressure, we need to understand pressure dependence of the two mechanisms, which will be described in the Discussion section. In the following section, we will determine the $H - P$ phase diagram of supercooling, superheating, and kinetic arrest temperatures, which will reveal how pressure affects the basic parameters of FOMT in these two contrasting systems.

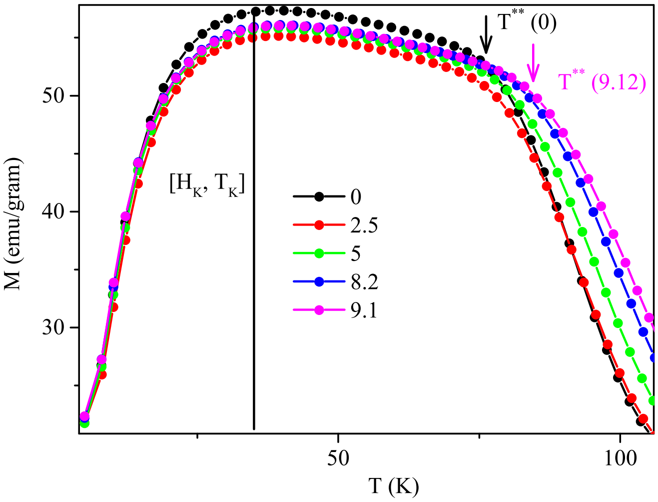

FIG. 6. ZFC curves of PCMAO at different P. The measurement $H = 5$ T. The vertical line marks the end of KA band. It indicates that $[H_K, T_K]$ remains unaffected by P.

B. Effect of pressure on the supercooling, superheating, and kinetic arrest temperatures

Thermal hysteresis in PCMAO progressively shifts toward higher temperature as P increases [see Fig. 3(a)], i.e., the supercooling (T^*) and superheating (T^{**}) temperatures increase with P. We want to mention here that we have performed magnetization measurements at different P and H, and can be found in the Supplemental Material [40]. Some data on LCMO can be found in Ref. [28]. The variation of the T^* and T^{**} with H and P are shown in Figs. 5(a) and 5(b). There are different ways to define T^* and T^{**} because the thermal hysteresis is broad. In case of PCMAO, we have considered the temperature where the (dM/dT) in FCC (FCW) shows the minima as T^* (T^{**}). In the FCC curve, M starts to increase rapidly at T_{NC}, which indicates the rapid nucleation and growth of the FM phase below T_{NC}. Similarly, in the FCW curve, nucleation of the AFM phase has started above T_{NW}. Interestingly, note that $T_{\mathrm{NC}} > T_{\mathrm{NW}}$, which means that onset of the nucleation of the AFM phase during heating has started at a lower temperature than the onset temperature of nucleation of FM phase during cooling. This indicates towards a wide distribution of the T^* and T^{**} in the material, such that they form bands instead of lines in $H - T$ plane, and overlap with each other. This occurs due to presence of quenched disorder, which results into a landscape of the transition temperature, and thereby broadening of the first-order transition [3,23]. In LCMO, the thermal hysteresis shifts towards lower temperature as higher P is applied. In this case, we have taken a different approach to find out the T^* and T^{**} values. In the FCC curve, the temperature where M shows peak, i.e., M as maximum is taken as the T^*. Similarly, T^{**} has been taken where M has a peak in the FCW curve. We have shown the variation of T^* and T^{**} in Figs. 5(c) and 5(d). The effect on T^* by P and H is quite dramatic in case of LCMO. T^* falls sharply at very tiny pressure of $P = 0.68$ kbar [Fig. 5(c)], remains comparatively unaffected at higher pressure. It is important to note that there are a few common features if we compare the effect of pressure on PCMAO and LCMO. First of all, application of P suppresses the AFM phase in both the systems, which is evident from the variation of T^* and T^{**} with pressure. Second, the variations of these transition temperatures are not linear in P.

Aside from T^* and T^{**}, the temperature T_K corresponding to kinetic arrest band is also important in the case of both PCMAO and LCMO. The phase coexistence persists even below the thermal hysteresis down to lowest temperature due to kinetic arrest band $[H_K, T_K]$ and, therefore, it is necessary to check the position of the $[H_K, T_K]$ band at higher pressure. In case of PCMAO, the effect of P on the $[H_K, T_K]$ band at a fixed H can be found from the measurement of the ZFC curves as shown in Fig. 6 [41]. In the case of zero-field cooling, as T is increased, magnetization sharply increases with temperature due to transformation of arrested AFM phase into the FM phase, which is called dearrest. M increases up to the end point of $[H_K, T_K]$ band, where the value of M is maximum, which we have marked as vertical line in Fig. 6. Note that this temperature is not significantly affected by pressure. Above this temperature, no significant conversion of the phase fraction happens until [H^{**}, T^{**}] band is reached, where the FM phase converts into AFM phase and M sharply decreases. We have also indicated the T^{**} values by the downward arrows for the ambient and highest applied pressures. These data reveal that the external pressure does not affect the [H_K, T_K] band significantly as compared to the [H^{**}, T^{**}] band. It should be mentioned here that [H_K, T_K] is practically a band, i.e., it is spread over certain $H - T$ window and the ZFC curve as shown Fig. 6 only gives one end of the band. Nonetheless, it can be shown that pressure does not significantly affect the width of the band as well (data not shown here). In case of LCMO also, P does not affect the [H_K, T_K] band significantly. The data have not been shown here for conciseness.

C. Effect of pressure on the nucleation and growth across the thermal hysteresis

A first-order transition during cooling proceeds through the nucleation and subsequent growth of the low-T phase at the cost of the high-T parent phase. Therefore, in case of PCMAO, as we gradually reduce the sample temperature, the high-T AFM phase transforms into the FM phase through the creation and growth of the FM droplets which are larger than a critical size [42]. This is manifested as the increase in M with decrease in temperature across the thermal hysteresis shown in Figs. 2(a) and 3(a). To investigate the effect of pressure on the kinetics across thermal hysteresis, we have measured isothermal relaxation of M with time at a fixed T in the hysteresis region, and at different P. We have recorded the time dependence of M in the field-cooled state, i.e., the sample has been cooled to the probing temperature in presence of the field and after stabilizing the temperature, magnetization has been recorded for the next few hours at the same field. The data have been shown in Fig. 7(a) for $T = 65$ K at $H = 4$ T. First of all, note that M increases with time, which confirms that high-T AFM phase transforms into the FM phase during cooling across the hysteresis region, which is expected. Now the important observation is, as P increases the relaxation rate, i.e., how fast M changes with time, becomes slower, which indicates that the growth rate of the FM phase fraction decreases at higher pressure.

Similarly, in LCMO, the transition during cooling proceeds through the transformation of the high-T FM phase into the low-T AFM phase. In Fig. 7(b), we have also shown the time dependence of M after the sample has been cooled in the field-cooled protocol to $T = 100$ K in presence of $H = 6$ T, which is within the thermal hysteresis region. We have followed identical protocol to measure $M(t)$ curves as in the case of PCMAO [Fig. 7(a)]. In this case also, the transformation rate reduces at higher pressure, and hence conforms that P suppresses the transformation rate from FM to AFM phase across the thermal hysteresis.

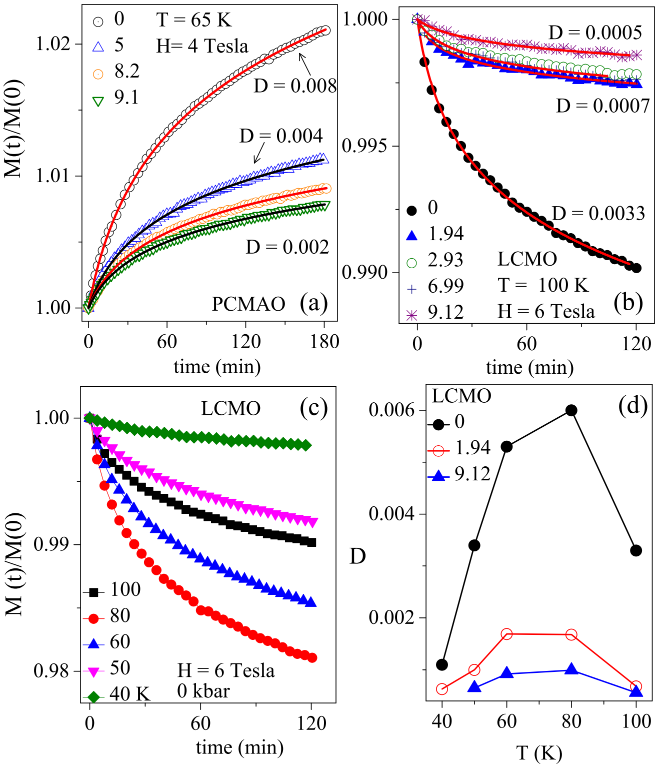

FIG. 7. Variation of M with time (a) of PCMAO at $T = 65$ K (b) of LCMO at 40 K measured in the FC protocol. The measurement fields are $H = 4$ and 6 T for PCMAO and LCMO, respectively. Solid lines are fitted curves using Eq. (2). D is the rate constant. The legends are the P values in the unit of kbar (c) the relaxation of M at various temperatures across the thermal hysteresis at $H = 6$ T and $P = 0$ in the FC protocol. The legends indicate the measurement temperatures. The curves are fitted using Eq. (2) and temperature dependence of D is shown in (d). It also presents the $D(T)$ at higher P. The solid lines in (d) are guide to eye.

Now, we will probe the effect of pressure on the metastable behavior across the entire thermal hysteresis region in case of LCMO. In Fig. 7(c), we have shown the time dependence of M (relaxation) at different temperatures within $T =$ 100 to 40 K at ambient pressure and $H = 6$ T which is the thermal hysteresis region. To measure these relaxation curves, we have followed similar protocol. The sample is cooled from room temperature (i.e., paramagnetic state) to the measurement temperatures in presence of the $H = 6$ T magnetic field. After the temperature becomes stable, magnetization has been recorded for next few hours without changing the field. First of all note that M decreases with time at all the temperatures because the high-T FM phase transforms into the AFM phase. Now, the change of M with time, i.e., the relaxation rate initially increases as we reduce the temperature from 100 K. For example, the relaxation at $T = 80$ K is faster than at 100 K. However, the relaxation again decreases with further decrease in the temperature down to 40 K. The increase in the relaxation rate with decreasing temperature can be understood in the framework of kinetically arrested first-order transition [27,32]. As temperature reduces, the free-energy barrier between the high- and low-T phases decreases, which results into the initial increase in the transformation rate [27,43]. However, the suppression of the relaxation rate on further reduction of temperature can be understood by the interplay between kinetic arrest and the free-energy landscape [27,32]. The relaxation curves can be satisfactorily described by logarithmic dependence of M on time, which is given by

$$M(t) = M(0)[1 + D \log(1 + t/\tau)]. \tag{2}$$

Here, $M(0)$ is the magnetization at time $t = 0$, and D is known as the rate constant which defines the relaxation rate or the viscosity coefficient [29,44–49]. Such logarithmic function has been successfully used earlier to investigate the metastable behavior of the nonequilibrium state in spin glasses, structural glasses, magnetic glass, etc. [29,45–48]. We have fitted all the time dependence of M data in Figs. 7(a) and 7(b) using Eq. (2). We have shown the fitted curves as the solid lines and mentioned the D values in the respective figures. As can be observed here, in both PCMAO and LCMO, D decreases with increasing P which further confirm that higher pressure inhibits the growth dynamics of the low-temperature phases in both the systems in the course of the FM-AFM first-order transition. Similarly, we have fitted the relaxation curves at various temperatures which are shown in Fig. 7(c) for ambient P and plotted the obtained D values in Fig. 7(d) (black filled circles). Also, we have measured the relaxation of M at higher pressure, but we have not shown here for conciseness. We have fitted those data by using Eq. (2) and plotted only the D values at a few selected higher P in Fig. 7(d). The variation of D with temperature at different P is qualitatively similar. But, quantitatively, it is evident that external P suppresses the growth rate in the entire temperature range of thermal hysteresis.

D. Effect of pressure on the transformation kinetics in the magnetic glass state

In the magnetic glass state, the nonequilibrium high-T phase which persists because of the KA gradually transforms into the equilibrium phase with time. The rate of transformation depends on the H and T. In Figs. 8(a) and 8(b), we have shown the change in M as a function of time at temperatures $T = 25$ and 40 K following field-cooled (FC) protocol in PCMAO and LCMO, respectively. To record the $M(t)$ curves, the sample is initially cooled from $T = 320$ K to the measurement temperatures at different P in presence of the cooling fields of $H = 4$ and 6 T for PCMAO and LCMO, respectively. After temperature becomes stable, M has been recorded as a function of time for the next few hours without changing the temperature and field. The thermal hysteresis at $H = 4$ and 6 T in PCMAO and LCMO close at $T = 30$ and 56 K, respectively [40]. Therefore, the measurement temperatures lie below the closer of the thermal hysteresis and situate in the magnetic glass regime of the respective materials. In case of conventional first-order transition, below the closer of the thermal hysteresis magnetization should not have any time dependence because there should not be any phase coexistence. However, as mentioned earlier in PCMAO and LCMO the coexistence of FM and AFM phases can persist due to kinetic arrest of the transition. The relaxation of M with time as observed in Figs. 8(a) and 8(b) indicates the nonequilibrium nature of the low-T state which can not be described in the framework of the metastable supercooled high-T phase. Note that in case of PCMAO [Fig. 8(a)], $M(t)$ increases with time at ambient P which indicates that the AFM phase is unstable at this temperature and it transforms to the equilibrium FM phase. As P increases, the increase in M with time, i.e., the relaxation rate monotonically decreases. It implies that the transformation rate monotonically reduces with the increase in P.

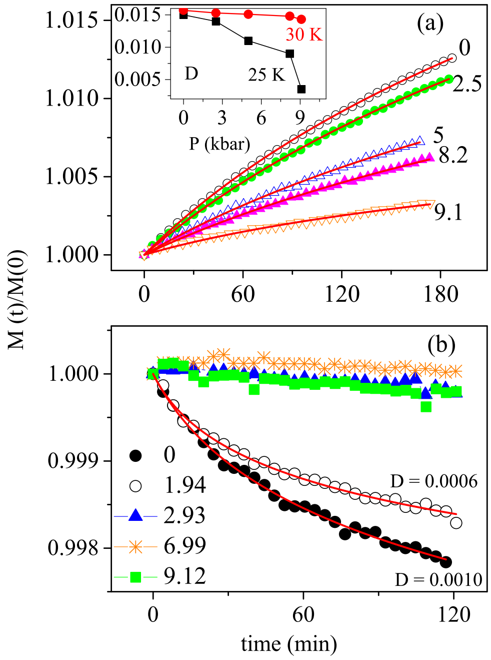

FIG. 8. Relaxation in the magnetic glass state in (a) PCMAO measured at $T = 25$ K and $H = 4$ T and (b) LCMO measured at $T = 40$ K and $H = 6$ T. Solid lines are the fitted curves using Eq. (2). The inset of (a) shows the D values at different P at $T = 25$ and 30 K in PCMAO obtained from fitting. The solid line in the inset is guide to eye. For LCMO, the curves at $P = 0$ and 1.94 kbar are fitted using the same equation.

On the other hand, in case of LCMO, the M decreases with time. It means that here the FM phase is the unstable phase and it gradually transforms into the equilibrium AFM phase. In this case, as P increases, the relaxation rate strongly decreases and becomes negligible at higher P. Therefore, P stabilizes the phase coexisting state in both the systems because it suppresses the relaxation rate of the FM-AFM transformation. However, at this field and temperatures, the suppression of the relaxation rate by P is pronounced in LCMO, compared to PCMAO. The relaxation curves can be fitted by using Eq. (2). We have mentioned the obtained D values for PCMAO in the main panel of Fig. 8(a). In the inset, we have shown the variation of D with P at $T = 30$ and 25 K. At $T = 30$ K, P suppresses the relaxation and D decreases with increase in P. However, the effect of P is more pronounced at $T = 25$ K, which indicates that P strongly suppresses the transformation kinetics at lower temperatures. D values for LCMO at $P = 0$ and 1.94 kbar have been mentioned in Fig. 8(b). At higher P, there is no appreciable relaxation of M.

V. DISCUSSION

In case of PCMAO, P monotonically increases the supercooling and superheating temperatures which indicate that P favors the FM phase. However, P does not significantly affect the $[H_K, T_K]$ band. It implies that the temperature window, where the first-order transition occurs before it is arrested, expands with increasing P. This should increase the equilibrium FM volume fraction at low temperature, say $T = 5$ K. However, the transformation rate from the high-T AFM to the low-T FM phase across the thermal hysteresis is simultaneously suppressed by P [see Fig. 7(a)]. Therefore, two competing mechanisms acting together decide the phase fraction of the competing phases at any temperature. The variation of volume fraction of the FM phase at $T = 5$ K indicates that initially the second mechanism must be dominating over the first, so that the FM phase fraction initially decreases at low P but finally increases, when the first mechanism dominates. Note that, because of these two competing interactions, the change in the volume fraction with pressure is also small. On the other hand, in case of LCMO, T^* reduces with increasing P and the T_K band is unchanged. Hence, the temperature window where the first-order transition from the high-T FM to low-T AFM phase occurs reduces with the increase in P. In addition, the nucleation and growth of the AFM phase is also suppressed by P. Therefore, both of these mechanisms together should result into the increase in the FM phase fraction at $T = 5$ K, which is observed in Fig. 3(b). Note that, in this case the change in the volume fraction is very large, which further supports this scenario.

We would like to mention here that in PCMAO, the suppression of the transformation rate from the high-T AFM to low-T FM phase across the thermal hysteresis [see Fig. 7(a)] by P is nontrivial. Because, as P increases the transition temperatures, the size of the critical nucleus of the FM phase at a particular temperature should be smaller at higher P [43,50]. This should, in principle, increase the growth rate of the FM phase, which is not the case in experiment. We believe that this contradiction can be understood from the extremely different spin structure of the FM and AFM phases in PCMAO. In the course of the transition, the nucleus of FM phase having a critical size (R_C) grows in the matrix of CE-AFM phase. At the interface, the two extremely different kinds of spin structure coexist, and hence are expected to have considerable spin disorder. It is possible that this disorder leads to strong interfacial frustration and causes hindrance to growth. Now, with increase in P the R_C decreases and, hence, the number of the FM nucleus as well as the interface between FM-AFM phases will increase. It is possible that the increase in the interface area suppresses the growth rate of the FM phase at higher P. Note that, in LCMO, where AFM is also CE type and grows within the FM matrix, the transformation rate decreases with P. The similar thing has been observed at low temperatures, i.e., in the magnetic glass state below thermal hysteresis [see Figs. 8(a) and 8(b)]. In PCMAO, the transformation from the AFM to FM phase at $T = 30$ K is suppressed by P, whereas, in LCMO the transformation from FM to AFM is hindered by P at $T = 65$ K. This reveals that higher P suppresses the transformation kinetics of the phase coexisting state in both systems. Basically, the growth of one phase in the matrix of the other phase appears to be suppressed at the interface of FM and CE-AFM. It is an open question as to how the unique spin-charge-orbital order of the CE-type AFM phase plays its role in controlling the frustration at the interface [51].

Nonetheless, the importance of the AFM-FM interface is evident from the observation of significant horizontal shift of the field-cooled $M - H$ loop in the phase coexistence region of both PCMAO and LCMO. Such shift in the $M - H$ loop is popularly known as the exchange bias, and occurs due to pinning of the surface spins at the interface [52]. In Fig. 9(a), we have compared isothermal variation of magnetization with field ($M - H$ curves) of PCMAO recorded after the samples have been cooled down to $T = 2$ K once in ZFC condition and then in presence of $H = 2$ T (FC $M - H$), and the field cycle has been performed between ±4 T. Similarly, Fig. 9(b) presents the the $M - H$ curves of LCMO at $T = 2$ K in both ZFC and FC conditions. In case of FC, the sample has been cooled at $H = 1$ T to $T = 2$ K, and the loop has been recorded between ±3 T. In Figs. 9(c) and 9(d), we have shown the expanded view of the hysteresis loops near the origin in both ZFC and FC $M - H$ loops of PCMAO and LCMO, respectively, which shows that the loop is not symmetric with respect to origin along the field axis when the $M - H$ loops have been measured in the FC conditions. It is shifted towards the negative field axis. The exchange-bias defined as $H_{\mathrm{EB}} = |(H_{C1} + H_{C2})|/2$, where H_{C1} and H_{C2} are the coercive fields along the positive and negative field axes, respectively. In case of PCMAO and LCMO, the H_{EB} has been found to be around $H_{\mathrm{EB}} \sim 350$ and 245 Oe, respectively. Such a shift in the hysteresis loop arises due to coexistence of the FM and AFM volume fractions in the close proximity with each other.

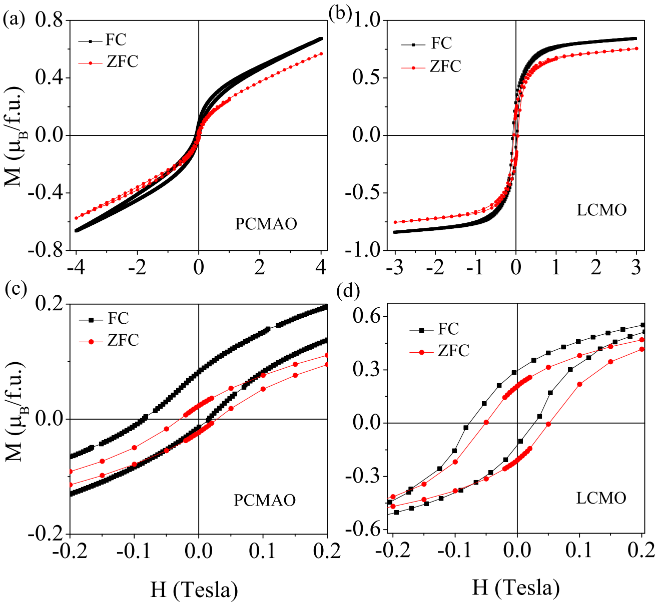

FIG. 9. (a) Isothermal ZFC and FC $M - H$ loops of PCMAO at $T = 2$ K. In the FC protocol, the sample has been cooled at $H = 2$ T, and the hysteresis loop has been measured between ± 4 T. (b) Isothermal ZFC and FC M-H loops of LCMO at $T = 2$ K. In case of FC M-H, the sample has been cooled at $H = 1$ T, and the hysteresis loop has been measured between ± 3 T. The expanded view of the loops of (c) PCMAO and (d) LCMO, near origin.

VI. SUMMARY

In brief, we have studied the effect of hydrostatic pressure on first-order magnetostructural phase transition under magnetic field. Two prototype systems PCMAO and LCMO with contrasting magnetic ground states have been investigated. We have performed our measurements in two different regions: (i) across thermal hysteresis, where phase coexistence occurs due to disorder broadening of first-order transition, and (ii) below the thermal hysteresis where kinetic arrest of the transition is responsible for the phase coexistence. We found that the volume fraction of the two coexisting phases and the supercooling and superheating temperatures can be tuned by applying external pressure, and how much the pressure is effective crucially depends on the applied magnetic field. Finally, we argue that at the interface of the two coexisting contrasting phases, the mismatch of the magnetic and crystal structure gives rise to strong interfacial frustration, which hinders the kinetics of the phase transformation at higher pressure in both systems.

[1] E. Dagotto, *Nanoscale Phase Separation and Colossal Magnetoresistance: The Physics of Manganites and Other Related Compounds* (Springer, Berlin, 2002).

[2] K. H. Ahn, T. Lookman, and A. R. Bishop, Strain-induced metal-insulator phase coexistence in perovskite manganites, Nature (London) **428**, 401 (2004).

[3] S. B. Roy, G. K. Perkins, M. K. Chattopadhyay, A. K. Nigam, K. J. S. Sokhey, P. Chaddah, A. D. Caplin, and L. F. Cohen, First order magnetic transition in doped $CeFe_2$ alloys: Phase coexistence and metastability, Phys. Rev. Lett. **92**, 147203 (2004).

[4] E. Dagotto, Complexity in strongly correlated electronic systems, Science **309**, 257 (2005).

[5] H. Lin, H. Liu, L. Lin, S. Dong, H. Chen, Y. Bai, T. Miao, Y. Yu, W. Yu, J. Tang *et al.*, Unexpected intermediate state photoinduced in the metal-insulator transition of submicrometer phase-separated manganites, Phys. Rev. Lett. **120**, 267202 (2018).

[6] Y. Zhu, K. Du, J. Niu, L. Lin, W. Wei, H. Liu, H. Lin, K. Zhang, T. Yang, Y. Kou *et al.*, Chemical ordering suppresses large-scale electronic phase separation in doped manganites, Nat. Commun. **7**, 11260 (2016).

[7] K. Zhang, K. Du, H. Liu, X.-G. Zhang, F. Lan, H. Lin, W. Wei, Y. Zhu, Y. Kou, J. Shao *et al.*, Manipulating electronic phase separation in strongly correlated oxides with an ordered array of antidots, Proc. Natl. Acad. Sci. USA **112**, 9558 (2015)

[8] N. K. Pandey, R. P. S. M. Lobo, and R. C. Budhani, Electric-field-tuned metallic fraction and dynamic percolation in a charge-ordered manganite, Phys. Rev. B **67**, 054413 (2003).

[9] J. Lourembam, J. Wu, J. Ding, W. Lin, and T. Wu, Electric field tuning of phase separation in manganite thin films, Phys. Rev. B **89**, 014425 (2014).

[10] S. K. Song and Han W. Yeom, Atomistic origin of metal versus charge-density-wave phase separation in indium atomic wires on Si(111), Phys. Rev. B **104**, 035420 (2021).

[11] W. Yang, Q. Shi, T. Miao, Q. Li, P. Cai, H. Liu, H. Lin, Y. Bai, Y. Zhu, Y. Yu *et al.*, Achieving large and nonvolatile tunable magnetoresistance in organic spin valves using electronic phase separated manganites, Nat. Commun. **10**, 3877 (2019).

[12] Seung S. Hong, M. Gu, M. Verma, V. Harbola, Bai Y. Wang, D. Lu, A. Vailionis, Y. Hikita, R. Pentcheva, J. M. Rondinelli *et al.*, Extreme tensile strain states in $La_{0.7}Ca_{0.3}MnO_3$ membranes, Science **368**, 71 (2020).

[13] C. P. Bean and D. S. Rodbell, Magnetic disorder as a first-order phase transformation, Phys. Rev. **126**, 104 (1962).

[14] M. Baldini, Y. Ding, S. Wang, Y. Lin, C. A. Tulk, A. M. dos Santos, J. F. Mitchell, D. Haskel, and W. L. Mao, Pressure-induced tuning of a magnetic phase separation in $Nd_{0.53}Sr_{0.47}MnO_3$, Phys. Rev. B **86**, 094407 (2012).

[15] A. S. McLeod, E. van Heumen, J. G. Ramirez, S. Wang, T. Saerbeck, S. Guenon, M. Goldflam, L. Anderegg, P. Kelly, A. Mueller *et al.*, Nanotextured phase coexistence in the correlated insulator V_2O_3, Nat. Phys. **13**, 80 (2017).

[16] Ka. H. Hong, Angel M. Arevalo-Lopez, J. Cumby, Clemens Ritter, and J. P. Attfield, Long range electronic phase separation in $CaFe_3O_5$, Nat. Commun. **9**, 2975 (2018).

[17] J. Sklenar, Y. Lao, A. Albrecht, Justin D. Watts, C. Nisoli, G.-W. Chern, and P. Schiffer, Field-induced phase coexistence in an artificial spin ice, Nat. Phys. **15**, 191 (2019).

[18] O. G. Udalov and I. S. Beloborodov, Tuning the magnetic state in a phase-separated magnetic oxide thin film by means of electric field and temperature, Phys. Rev. B **101**, 174433 (2020).

[19] G. Zhou, H. Ji, W. Lin, J. Zhang, Y. Bai, J. Chen, M. Wu, and X. Xu, Orbital reconstruction mediated giant vertical magnetization shift and insulator-to-metal transition in superlattices based on antiferromagnetic manganites, Phys. Rev. B **101**, 024422 (2020).

[20] S. B. Roy, First order magneto-structural phase transition and associated multi-functional properties in magnetic solids, J. Phys.: Condens. Matter **25**, 183201 (2013).

[21] V. Markovich, I. Fita, A. Wisniewski, R. Puzniak, C. Martin, G. Jung, and G. Gorodetsky, Phase transitions and magnetic properties of $LuFe_2O_4$ under pressure, Phys. Rev. B **96**, 054416 (2017).

[22] S. Banik, K. Das, T. Paramanik, Niranjan P. Lalla, B. Satpati, K. Pradhan, and I. Das, Huge magnetoresistance and ultrasharp metamagnetic transition in polycrystalline $Sm_{0.5}Ca_{0.25}Sr_{0.25}MnO_3$, NPG Asia Mater. **10**, 923 (2018).

[23] Y. Imry and M. Wortis, Influence of quenched impurities on first-order phase transitions, Phys. Rev. B **19**, 3580 (1979).

[24] M. K. Chattopadhyay, S. B. Roy, and P. Chaddah, Kinetic arrest of the first-order ferromagnetic-to-antiferromagnetic transition in $Ce(Fe_{0.96}Ru_{0.04})_2$: Formation of a magnetic glass, Phys. Rev. B **72**, 180401(R) (2005).

[25] A. Banerjee, K. Mukherjee, K. Kumar, and P. Chaddah, Ferromagnetic ground state of the robust charge-ordered manganite $Pr_{0.5}Ca_{0.5}MnO_3$ obtained by minimal Al substitution, Phys. Rev. B **74**, 224445 (2006).

[26] A. Banerjee, K. Kumar, and P. Chaddah, Enhancement of equilibrium fraction in $La_{0.5}Ca_{0.5}MnO_3$ by recrystallization, J. Phys.: Condens. Matter **20**, 255245 (2008).

[27] P. Chaddah, K. Kumar, and A. Banerjee, Devitrification and recrystallization of magnetic glass $La_{0.5}Ca_{0.5}MnO_3$, Phys. Rev. B **77**, 100402(R) (2008).

[28] S. Dash, K. Kumar, A. Banerjee, and P. Chaddah, Effect of simultaneous application of magnetic field and pressure on magnetic transitions in $La_{0.5}Ca_{0.5}MnO_3$, Phys. Rev. B **82**, 172412 (2010).

[29] A. Banerjee, P. Chaddah, S. Dash, K. Kumar, A. Lakhani, X. Chen, and R. V. Ramanujan, History-dependent nucleation and growth of the martensitic phase in the magnetic shape memory alloy $Ni_{45}Co_5Mn_{38}Sn_{12}$, Phys. Rev. B **84**, 214420 (2011).

[30] K. Mukherjee, K. Kumar, A. Banerjee, and P. Chaddah, On the correlation between supercooling, superheating and kinetic arrest in a magnetic glass $Pr_{0.5}Ca_{0.5}Mn_{0.975}Al_{0.025}O_3$, Eur. Phys. J. B **86**, 21 (2013).

[31] S. Pal, K. Kumar, A. Banerjee, S. B. Roy, and A. K. Nigam, Non-equilibrium magnetic response of canonical spin glass and magnetic glass, J. Phys.: Condens. Matter **33**, 025801 (2021).

[32] S. Pal, K. Kumar, and A. Banerjee, Memorylike response of the magnetic glass, Phys. Rev. B **103**, 144434 (2021).

[33] W. Wu, C. Israel, N. Hur, S. Park, S.-W. Cheong, and A. de Lozanne, Magnetic imaging of a supercooling glass transition in a weakly disordered ferromagnet, Nat. Mater. **5**, 881 (2006).

[34] Y. J. Choi, C. L. Zhang, N. Lee, and S.-W. Cheong, Cross-control of magnetization and polarization by electric and magnetic fields with competing multiferroic and weak-ferromagnetic phases, Phys. Rev. Lett. **105**, 097201 (2010)

[35] X. F. Miao, Y. Mitsui, A. I. Dugulan, L. Caron, N. V. Thang, P. Manuel, K. Koyama, K. Takahashi, N. H. van Dijk, E. Brück *et al.*, Kinetic-arrest-induced phase coexistence and metastability in $(Mn, Fe)_2(P, Si)$, Phys. Rev. B **94**, 094426 (2016).

[36] A. K. Nayak, M. Nicklas, C. Shekhar, and C. Felser, Kinetic arrest related to a first-order ferrimagnetic to antiferromagnetic transition in the Heusler compound Mn_2PtGa, J Appl. Phys. **113**, 17E308 (2013).

[37] O. Cakir, E. Dias, K. R. Priolkar, A. Hoser, M. Farle, and M. Acet, Heterogeneous magnetism and kinetic arrest in antiperovskite $Mn_{3-x}Ni_xGaC$ compounds with Ni_2MnGa Heusler insertions, Phys. Rev. B **102**, 024431 (2020).

[38] P. Saha and R. Rawat, History dependent resistivity relaxation behavior of $FeRh_{0.46}Pd_{0.54}$ in H-T space, J. Magn. Magn. Mater. **509**, 166859 (2020).

[39] S. Nair and A. Banerjee, Formation of finite antiferromagnetic clusters and the effect of electronic phase separation in $Pr_{0.5}Ca_{0.5}Mn_{0.975}Al_{0.025}O_3$, Phys. Rev. Lett. **93**, 117204 (2004); The effect of Al substitution on charge ordered $Pr_{0.5}Ca_{0.5}MnO_3$: Structure, magnetism and transport, J. Phys.: Condens. Matter **16**, 8335 (2004).

[40] See Supplemental Material at http://link.aps.org/supplemental/10.1103/PhysRevB.108.214409 for detailed magnetization measurements at various magnetic fields and pressure.

[41] A. Lakhani, P. Kushwaha, R. Rawat, K. Kumar, A. Banerjee, and P. Chaddah, Field dependence of temperature induced irreversible transformations of magnetic phases in $Pr_{0.5}Ca_{0.5}Mn_{0.975}Al_{0.025}O_3$ crystalline oxide, J. Phys.: Condens. Matter **22**, 032101 (2010).

[42] R. Rawat, P. Kushwaha, D. K. Mishra, and V. G. Sathe, Direct visualization of first-order magnetic transition in $La_{5/8-y}Pr_yCa_{3/8}MnO_3$(y=0.45) thin films, Phys. Rev. B **87**, 064412 (2013).

[43] P. M. Chaikin and T. C. Lubensky, *Principles of Condensed Matter Physics* (Cambridge University Press, Cambridge, 1994).

[44] A. Amir, Y. Oreg, and Y. Imry, Slow relaxations and aging in the electron glass, Phys. Rev. Lett. **103**, 126403 (2009).

[45] S. Kustov, I. Golovin, M. L. Corr, and E. Cesari, Isothermal martensitic transformation in metamagnetic shape memory alloys, J. Appl. Phys. **107**, 053525 (2010).

[46] S. Pal, K. Kumar, and A. Banerjee, Probing metastability in oxygen deficient YMn_2O_5, in *DAE Solid State Physics Symposium 2016*, AIP Conf. Proc. No. 1832 (AIP, Melville, NY, 2017), p. 030022.

[47] S. Pal, K. Kumar, R. Sharma, A. Banerjee, S. B. Roy, J.-G. Park, A. K. Nigam, and S.-W. Cheong, Possible glass-like random singlet magnetic state in 1T-TaS_2, J. Phys.: Condens. Matter **32**, 035601 (2020).

[48] S. Pal and A. Banerjee, Finite size effect on the magnetic glass, J. Phys.: Condens. Matter **34**, 035801 (2022)

[49] M. Manekar, C. Mukherjee, and S. B. Roy, Imaging of time evolution of the first-order magneto-structural transition in Fe-Rh alloy using magnetic force microscopy, Europhys. Lett. **80**, 17004 (2007).

[50] P. Chaddah, S. Dash, K. Kumar, and A. Banerjee, Overtaking while approaching equilibrium, arXiv:1011.3598.

[51] H. Zhou, Q. Feng, Y. Hou, M. Nakamura, Y. Tokura, M. Kawasaki, Z. Sheng, and Q. Lu, Imaging the formation and surface phase separation of the CE phase, npj Quantum Mater. **6**, 56 (2021)

[52] J. Nogues and I. K. Schulle, Exchange bias, J. Magn. Magn. Mater. **192**, 203 (1999).